buildings

MDPI

Article

Seismic Strengthening of RC Structures Using Wall-Type Kagome Damping System

Moo-Won Hur, Yonghun Lee, Min-Jun Jeon and Sang-Hyun Lee *

Department of Architectural Engineering, Dankook University, Yongin-si 16890, Gyeonggi-do, Korea; hmw01@nate.com (M.-W.H.); lyn3040@naver.com (Y.L.); melody9170@naver.com (M.-J.J.)
* Correspondence: lshyun00@dankook.ac.kr; Tel.: +82-31-8005-3735

Abstract: In this study, the Kagome truss damper, a metallic wire structures, was introduced and its mechanical properties were investigated through theoretical analyses and experimental tests. The yield strength of the Kagome damper is dependent on the geometric shape and diameter of the metallic wire. The Kagome damper has higher resistance to plastic buckling as well as lower anisotropy. Cyclic shear loading tests were conducted to investigate the energy dissipation capacity and stiffness/strength degradation by repeated loadings. The hysteretic properties obtained from the tests suggest that a modification of the ideal truss model with a hinged connection could be used to predict the yield strength and stiffness of the damper. For seismic retrofitting of a low-rise RC moment frame system, a wall-type Kagome damping system (WKDS) was proposed. The effectiveness of the proposed system was verified by conducting cyclic loading tests using a RC frame with/without the WKDS (story drift ratio limit 1.0%). The test results indicated that both the strength and stiffness of the RC frame increased to the target level and that its energy dissipation capacity was significantly enhanced. Nonlinear static and dynamic analyses were carried out to validate that the existing building structure can be effectively retrofitted using the proposed WKDS.

Keywords: Kagome truss damper; wall-type Kagome damping system; seismic retrofit; cyclic loading tests

check for updates

Citation: Hur, M.-W.; Lee, Y.; Jeon, M.-J.; Lee, S.-H. Seismic Strengthening of RC Structures Using Wall-Type Kagome Damping System. *Buildings* **2022**, *12*, 41. https://doi.org/10.3390/buildings12010041

Academic Editor: Alessandra Aprile

Received: 22 November 2021
Accepted: 23 December 2021
Published: 4 January 2022

Publisher's Note: MDPI stays neutral with regard to jurisdictional claims in published maps and institutional affiliations.

Copyright: © 2022 by the authors. Licensee MDPI, Basel, Switzerland. This article is an open access article distributed under the terms and conditions of the Creative Commons Attribution (CC BY) license (https://creativecommons.org/licenses/by/4.0/).

1. Introduction

Non-seismically designed low-rise RC building structures are vulnerable to earthquakes, which has been confirmed by the devastating damages to RC frame buildings caused by the Kobe (1995), Chi-Chi (1999), Izmit (1999), Sichuan (2008), and L'Aquila (2009) earthquakes [1–5]. Over the last few decades, extensive research has been conducted with the aim of improving the non-seismically designed RC frame, and many different damping devices have been introduced as attractive alternatives for seismic retrofitting. For instance, a metallic yield damper employing the yielding mechanism of the steel material is the most widely used hysteretic damper due to its low manufacturing cost and high energy dissipation capacity. Research on metallic yield dampers began in the early 1970s [6]. To ensure simultaneous yielding of the plates, X- or triangular-shaped steel plates were adopted as the main component of the metallic damper. Whittaker (1991) and Tsai (1992) showed that the metallic yield damper has stable hysteresis, durability, and temperature-independent properties [7,8]. The slit type metallic damper absorbs dynamic energy by flexural deformation of the parallel steel strips under in-plane shear force [9]. Conventional diagonal and Chevron type bracing systems have been used for damper installation. To increase the stable energy dissipation capacity, various types of metallic dampers and installation systems have been proposed.

Bincy, V. and Usha, S. (2021) proposed dual-pipe damper for seismic reinforcement improvement, and an optimization experiment was conducted while adjusting the number of pipes using the proposed dual-pipe damper [10]. Panumas Saingam et al. (2021)

proposed a combination seismic reinforcement method using viscous dampers and elastic steel frames. We demonstrate its effectiveness by performing performance experiments and numerical interpretations with the proposed method [11]. Ohad Idels and Oren Lavan (2021) have verified the optimization-based seismic design of steel moment resistance frames using the Scoss Damper through numerical analysis [12]. Farshad Taiyari et al. (2019) proposed a new bracing system with U-shaped elements as energy dissipation devices. This proposed bracing system can be considered as a hysteretic damper, which combines the advantages of yielding dampers and buckling resistant braces (BRB) [13]. Xuchuan Lin et al. (2018) developed a buckling suppression shear panel damper with a detachable steel concrete composite material system. A series of tests involving twelve specimens were conducted to examine the effects of the key design aspects on the seismic behavior [14]. Yamazaki S et al. (2016) presented a buckling-restrained rippled plate damper that can be used as the stiff elastic bearing in small earthquakes and as the energy dissipating damper in large earthquakes [15]. Tagawa H et al. (2016) proposed a seesaw energy dissipation system using a steel slit damper for the bracing to remain in tension during cyclic excitation [16]. Chan REK et al. (2015) developed a yielding shear panel device using a short segment of a square hollow section with a steel diaphragm plate welded inside [17]. The well-known buckling restrained brace (BRB) is for achieving stable energy hysteresis using the core steel members in which buckling is restrained by confining concrete. Generally, the dampers used in bracing systems only showed sound performance in cases involving unidirectional movements. To achieve multi-directional performance, a structural member with inherent multi-directionality or multiple unidirectional elements can be used. Infanti S et al. (2004) used a tapered pin as a seismic isolation system due to its inherent multi-directionality stemming from its symmetry [18]. Milani AS. and Dieleli M. (2015) proposed a multi-directional torsional hysteretic damper composed of eight hysteretic elements in a radial shape [19].

Kagome, which is a three-dimensional metallic wire structure, has been one of the convincing options to mitigate vibration in various fields such as mechanical engineering, naval architecture, and aerospace engineering. It is manufactured to be porous and has periodic cells by scaling a truss structure down to millimeter scale [20].

A wire truss, as is well known, is more lightweight than other structures, e.g., pyramid or octet type truss structures guaranteeing a similar level as them in bending and axial strengths. Kagome truss is fabricated by inserting and rotating spiral-shaped wires and fixing wire-crossing points to be three-dimensional structure [21]. Choi et al. (2008) and Lee et al. (2008) determined the elastic modulus and axial strength of a Kagome structure according to the diameter of wire and pitch ratio as design parameters [22,23]. Lee et al. (2009) carried out a series of compression tests on both convex and concave type Kagome truss to compare their axial strengths, and Park et al. (2010) presented the young's modulus and compressive strength of a Kagome truss according to the wire curvature [24,25]. In addition, Lee and Kang (2008) researched into the bending strength and behavior the wire-woven Kagome [26]. According to earlier studies by Hwang (2016), it is possible to identify the mechanical characteristics of the Kagome structure with particular emphasis on its compressive strength and bending behavior [27]. However, regarding the damping effect induced by shear strain, only a basic concept has been derived thus far. For it to be used as a damping device to suppress the seismic response of buildings, a numerical model of a Kagome damper must be developed to evaluate the shear hysteretic behavior concerning its energy dissipation capacity, and the most efficient installation system using braces or panels must be identified. As shown in Figure 1, unit cells of a Kagome damping device formed by small tetrahedrons and large octahedrons are arrayed regularly and steadily. Figure 2 shows the shear behavior of Kagome damping device. The Kagome damping device has an isotropic energy dissipation characteristic, which means the damping features are identical in two-axial direction. Also, the stiffness in the axial direction has greater stiffness than the X and Y-directions. These features also reduce vertical subsidence.

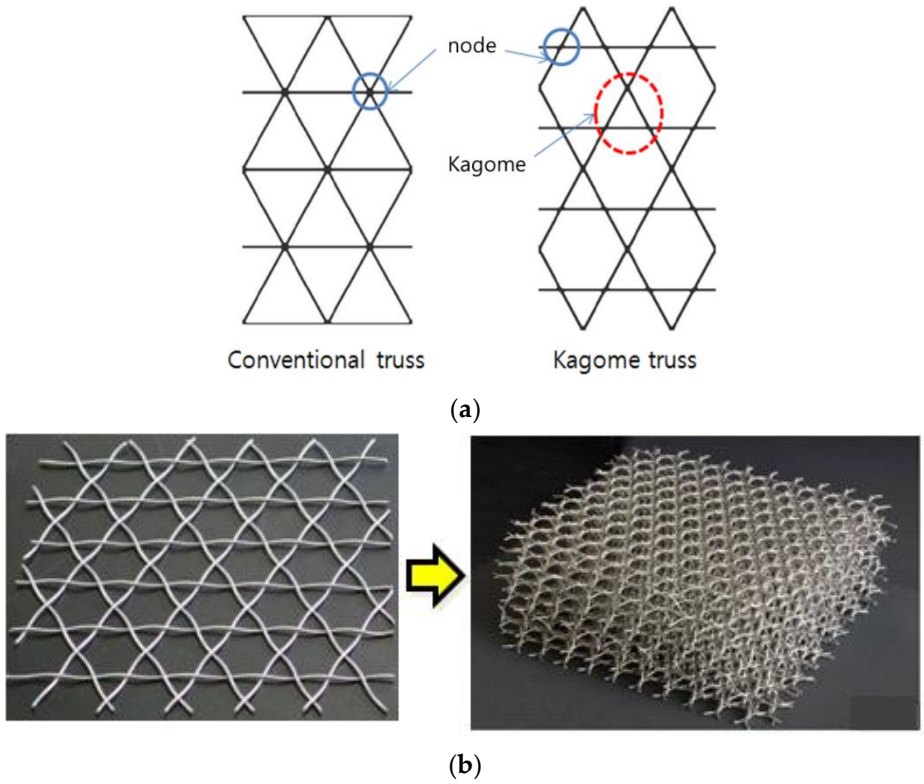

Figure 1. Kagome truss structures and the three-dimensional form [28]. (**a**) Comparison of general truss structure and Kagome structure. (**b**) Comparison of general truss structure and Kagome structure.

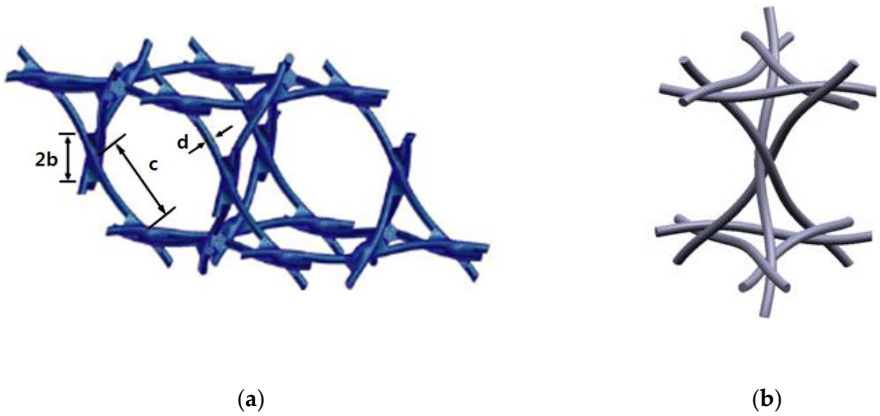

Figure 2. Shape of the Kagome damper unit cell [28]. (**a**) Unit cell, (**b**) Tetrahedron.

In this study, the seismic performance of the Kagome truss damper system is discussed for use in the vibration control of structures subjected to seismic excitation, and a structural model of the Kagome system is developed based on the experimentally obtained hysteretic behaviors. The yield and shear strengths, strain capacity, and stiffness are determined theoretically and experimentally. The wall-type Kagome damping system (WKDS) is proposed as an installation system for a moment frame. Cyclic loading tests are performed on single-bay and single-story reinforced concrete frames with and without the WKDS. Finally, nonlinear time history analyses are conducted for a four-story building structure with and without WKDS.

2. Kagome Damper and Wall-Type Kagome Damping System

2.1. Metal-Wire Kagome Truss Damper

The word, 'Kagome', came from the tri-hexagonal pattern which has been used to make Japanese folk baskets. Owing to the features that the truss members of the Kagome do not cross at a node (see Figure 1a), and it allows shortening of the truss members, Kagome is able to resist buckling effectively. Compared to the octet-truss or square pyramid, besides, the main material is still more lightweight thanks to the smaller number of truss members maintaining similar level of the mechanical capacity. As Figure 1b illustrates, the cross-sections of the Kagome damper composed of helical wires along six directions are fixed by brazing, and it is assembled vertically.

2.2. Properties of Idealized Shear Behavior

In this section, shear elastic modulus and shear strength are theoretically determined. In Figure 2 describing a unit cell of the Kagome damper resisting external loads, geometric variables c, d, and b denote length of the truss element, a diameter of a wire, and a height of a brazed joint. Simplifying the Kagome truss structure into an ideal form composed of the linear elements, the shear force in a unit cell can be properly estimated.

(1) Shear Elastic Modulus

Assuming that a unit cell subjected to compressive load Q and shear force R, and the member forces act as shown in Figure 3. Simplifying the truss structure into an ideal form, or two regular tetrahedrons (see Figure 3), the stiffness is written as

$$\frac{R}{\delta_R} = \frac{\pi d^2 E_w}{8c}, \tag{1}$$

where δ_R, E_w are the displacement of the tetrahedron in the direction of R and the elastic modulus of the wire respectively. The planar area of the tetrahedron in a unit cell A_o is $2\sqrt{3}c^2$, and the height of the tetrahedron H_o is $\sqrt{2/3}c$. Dividing load R by A_o and the displacement δ_R by H_o gives the shear elastic modulus G in the direction of R is determined as

$$G = \frac{\sqrt{2}}{48}\pi E_w \left(\frac{d}{c}\right)^2. \tag{2}$$

(2) Shear Strength

Supposing that the shear force R acts along the most critical direction as shown in Figure 3, from the geometric property of a regular tetrahedron, the member forces are

$$F_1 = -\frac{2}{\sqrt{3}}R, F_2 = \frac{1}{\sqrt{3}}R, F_3 = \frac{1}{\sqrt{3}}R, \tag{3}$$

where (–) indicates a compressive force. Dividing the yield load of the member 1, which is receiving the most axial force by the external shear force R, by the surface area of a unit cell gives the maximum shear stress written as

$$R_p = \frac{\pi \sigma_y}{16}\left(\frac{d}{c}\right)^2, \tag{4}$$

where σ_y denotes the yield strength of wire. As Equation (4), the length-depth ratio ($\lambda = c/d$) affects the shear stress. From Equations (2) and (4), the yield strain of a unit cell is determined as

$$\varepsilon_y = \frac{3}{\sqrt{2}}\frac{\sigma_y}{E_w}. \tag{5}$$

If the shear force acts as Figure 3 shows, the member is yielded at the shear stress, R_p (see Equation (4)). The unit cell, however, still be preserved by the tension of the two lasting truss members. Thus, it is expected that the force–displacement curve has a bi-linear form after yield of a member.

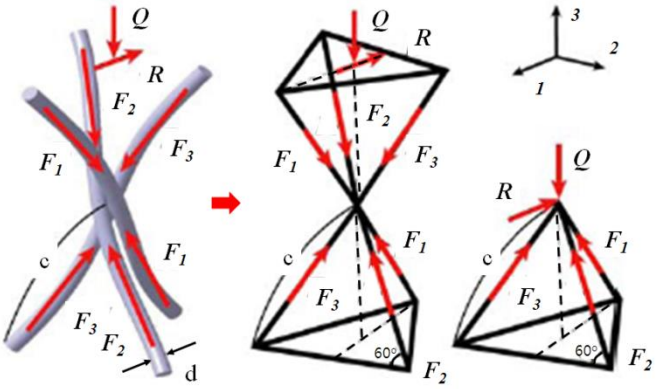

Figure 3. Ideal Kagome equivalent structures [28].

2.3. Model Structure and Test Specimen

Various installation systems for passive dampers have been presented, including conventional diagonal or K-bracing and toggle bracing. In this study, the wall-type installation system shown in Figure 4 was used in an attempt to minimize damage to the architectural façade. The WKDS are installed as anchors. There is a slab at the top of the beam where WKDS are installed to minimize damage to the beam due to the installation of WKDS.



(**a**)

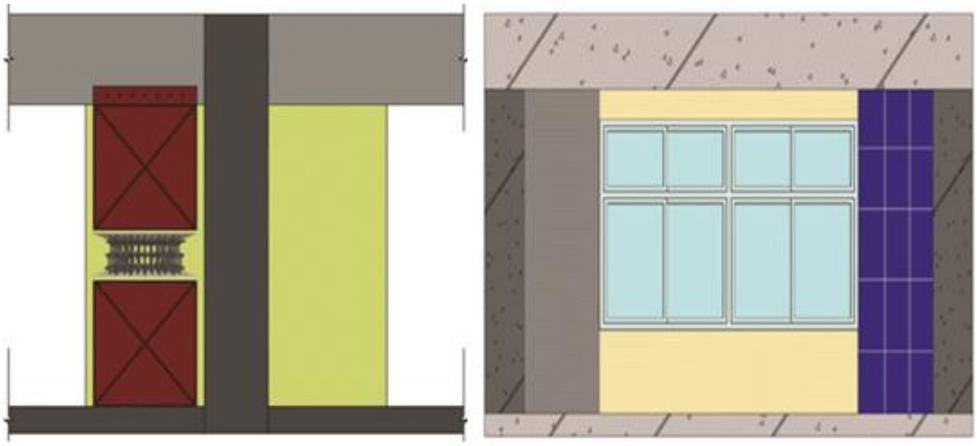

(**b**)

Figure 4. Wall-type Kagome damping system. (**a**) WKDS installation location, (**b**) WKDS construction.

As a case study to verify the seismic improvement of the WKDS, a series of cyclic loading tests was conducted with the RC frame structure, which was designed without considering earthquake loads. The target performance level is a 50% increase in the lateral

strength and a drift ratio of 1%. The building model used for the case study is a school in South Korea constructed in 1986. At that time, the seismic design code was not yet part of the Korean Building Code. A part of the exterior frame at the first story was selected to be strengthened by employing the Kagome damper, as shown in Figure 5.

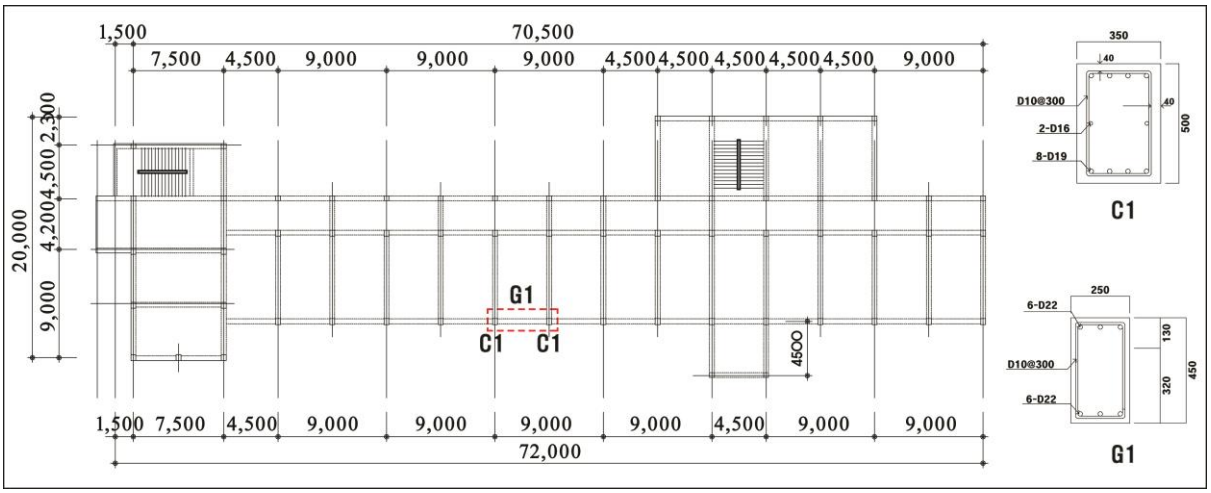

Figure 5. Plan view of the school building with the section used for testing shown in the dashed outline.

The scale of the test specimen was 60% of the actual frame size. Table 1 presents a comparisons of the dimensions of the existing original frame and the scaled-down specimen used for structural tests. When considering the size of the structural laboratory facility, actuator equipment, and the capacity of the overhead travelling crane, the ratio of the dimension reduction is 60% (Table 1).

Table 1. Comparison of members between original frame and test specimens.

Content	Full Scale	60% Scale	Remarks
Column	500 × 350 mm	300 × 210 mm	-
Story	3300 mm	1980 mm	Beam included
Axial load	5060 kN: (2530 kN/column)	180 kN (90 kN/column)	- One column area: (0.5 × 7.5) × (0.5 × 4.5) = 8.4 m^2 - One story axial load = 84 × 10 kN/m^2 (floor area unit weight): 84 kN - Total axial load: 84 × 3 actuator = 253 kN
Span	4500 mm	2700 mm	

Figure 6 illustrates the reinforcement placing in detail. The column size is 210 mm × 300 mm and the clear length of the column is 1680 mm. The dimensions of the main bars and the hoop bars are 10-D13 and D6@ 180, respectively. The compressive strength of the concrete is 20.53 MPa and the yield strength of the steel bars is 300 MPa (Table 2).

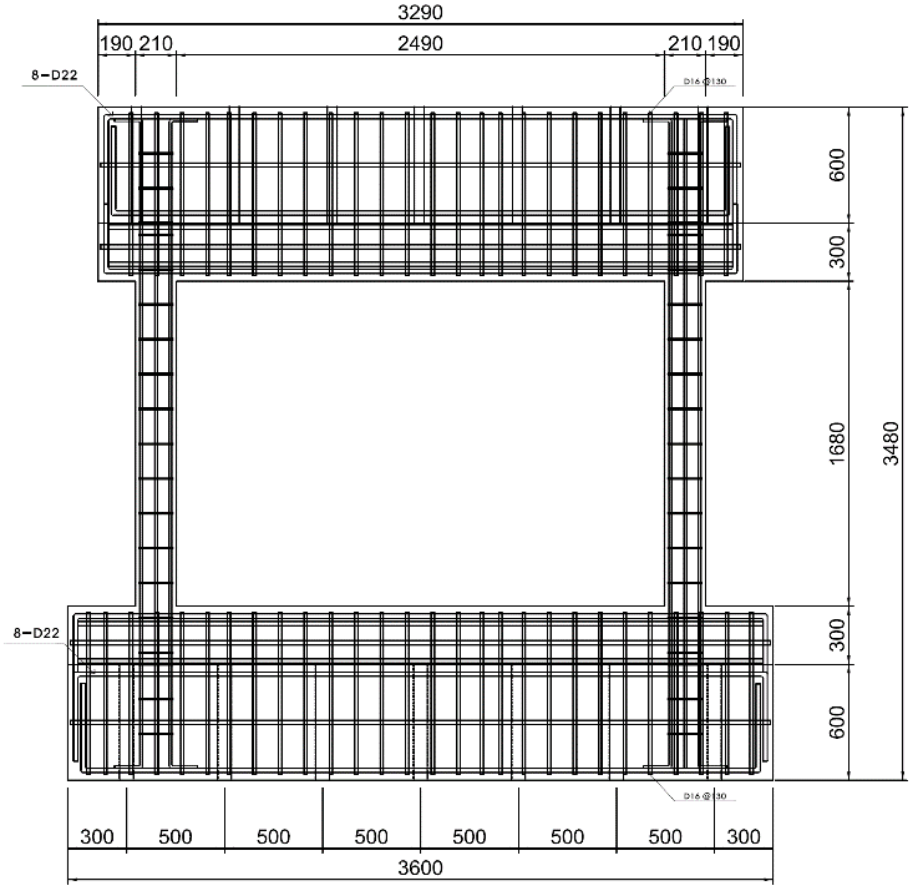

Figure 6. Reinforcement placing of the test specimen.

Table 2. Characteristic value of concrete and material properties of steel (unit: MPa).

No	Concrete Strength		Modulus of Elasticity	Bar Size	Yield Strength	Yield Strain ($\times 10^{-5}$)	Tensile Strength	Elongation (%)
	fck	fck. ave.						
1	20.45	20.53	1.96 × 104	D13	348.03	2960.3	517.41	36.0
2	21.21							
3	19.45			D10	299.55	4205.8	418.6	26.8
4	18.37							
5	22.56			12T	332.01	1919.0	477.3	26.8
6	21.12							

Figure 7 shows the configuration of the damper installation. Two identical steel walls sized 690 mm × 500 mm made of rectangular steel pipes were used as a rig for the Kagome damper between the upper and lower girder. The damper was positioned at the center between the steel walls such that the hysteresis of the damper was mainly governed by the shear deformation.

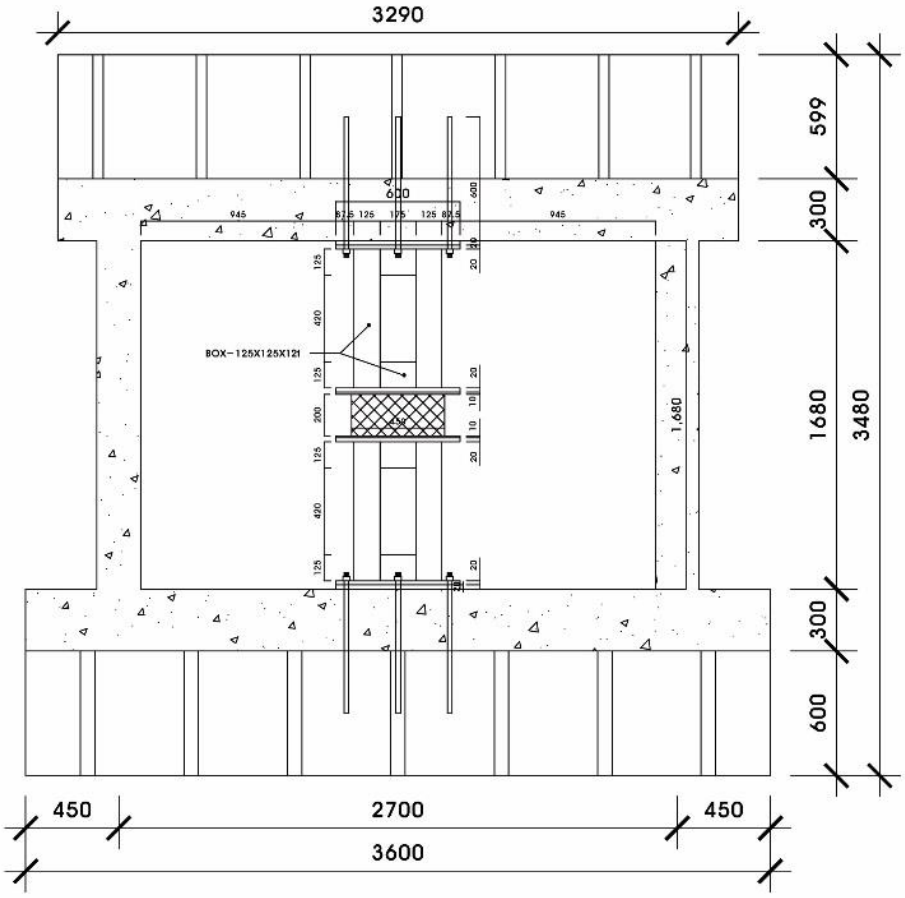

Figure 7. Installation of the Kagome damper.

2.4. Design of the Kagome Damper

Since the WKDS has higher initial stiffness and lower yield strength than the original structure, the WKDS can increase the energy dissipation capacity of the whole system earlier than the original RC structure can. The highest performance of the Kagome damper can be expected when the yield displacement of the damper is less than 25% of the yield displacement of the structure [29]. In this study, the Kagome damper was designed to yield at the 10% of the yield displacement of the structure. The pushover analysis result shown in Figure 8 indicates that the original structure had 6.7 mm yield displacement and 96 kN yield strength. Meanwhile, the displacement and strength at the yielding point of the Kagome damper were 0.67 mm and 50 kN, respectively.

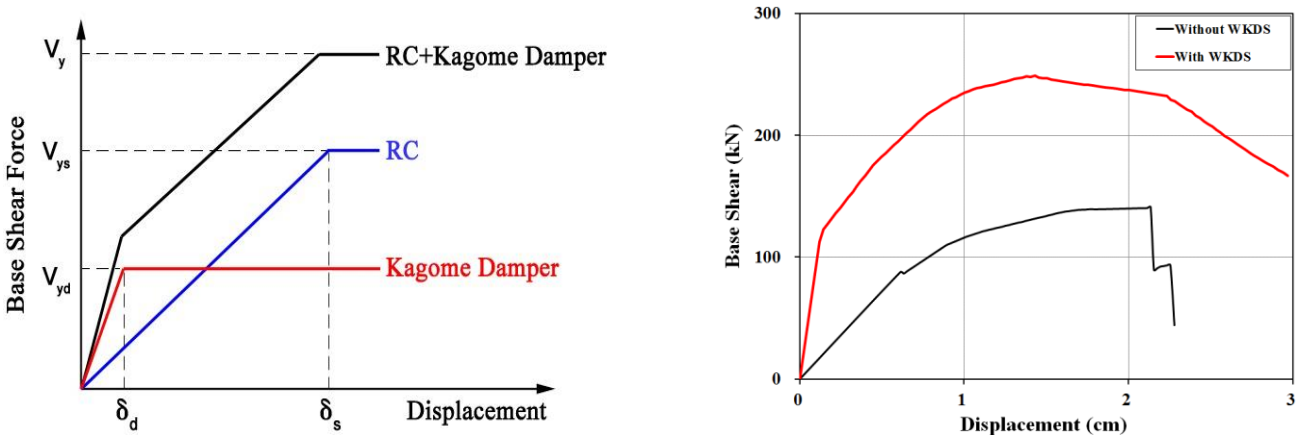

Figure 8. Base shears and displacements of structures with and without WKDS.

2.5. Test Setup

Figure 9 shows the test setup. The upper part of the test specimen is connected to a rigid steel frame connected to three actuators. During testing, the upper RC girder was subjected to a constant vertical load (258.3 kN($0.1P_u / A_g f_{ck}$)) to reproduce the effect of the axial load in the columns. The other actuator is for the cyclic lateral load, the protocol of which is described in Figure 10. The protocol planning was planned according to the method given in ACI 374.1. The first lateral displacement ($\delta(=\Delta/a)$) started from the elastic range $\delta = 0.08\%$. The lateral displacement ratio of the next stage was increased by 1.25 times the lateral displacement ratio of the previous stage. For each step, 3 cycles were applied. The test continued the force of the test until the strength decreased below 20%.



(**a**)



(**b**)

Figure 9. Test set-up. (**a**) without WKDS, (**b**) with WKDS.

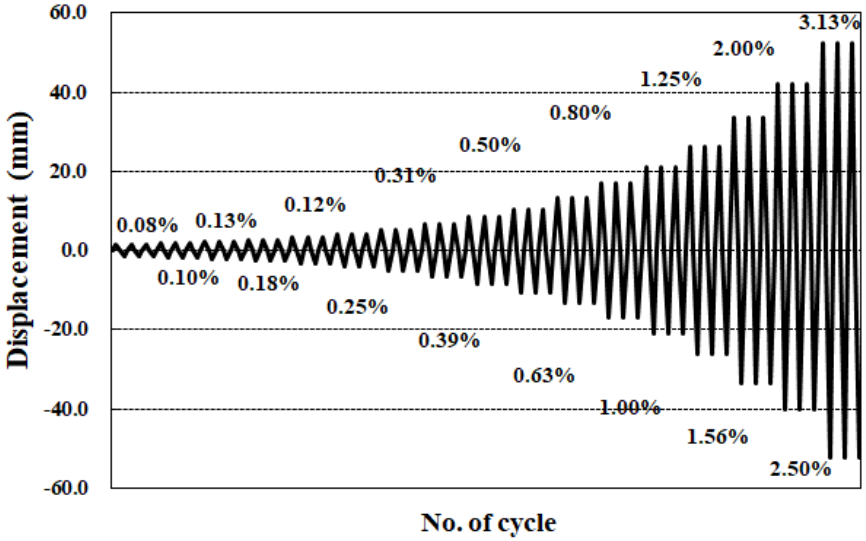

Figure 10. Cyclic loading protocol.

The actuator applying lateral load was displacement-controlled, exponentially increasing the displacement from 1.46 mm to 42.0 mm over sixteen steps; at each step, three cycles were repeated. Figure 11 illustrates the configuration of the measurement of linear variable differential transformers (LVDTs) and strain gages. Five LVDTs were installed to measure the displacement of the frame and two LVDTs were used to measure the deformation of the Kagome damper. Ten strain gages (C1~C10) were attached to the main bars and nine strain gages (S1~S9) were attached to the hoop bars.

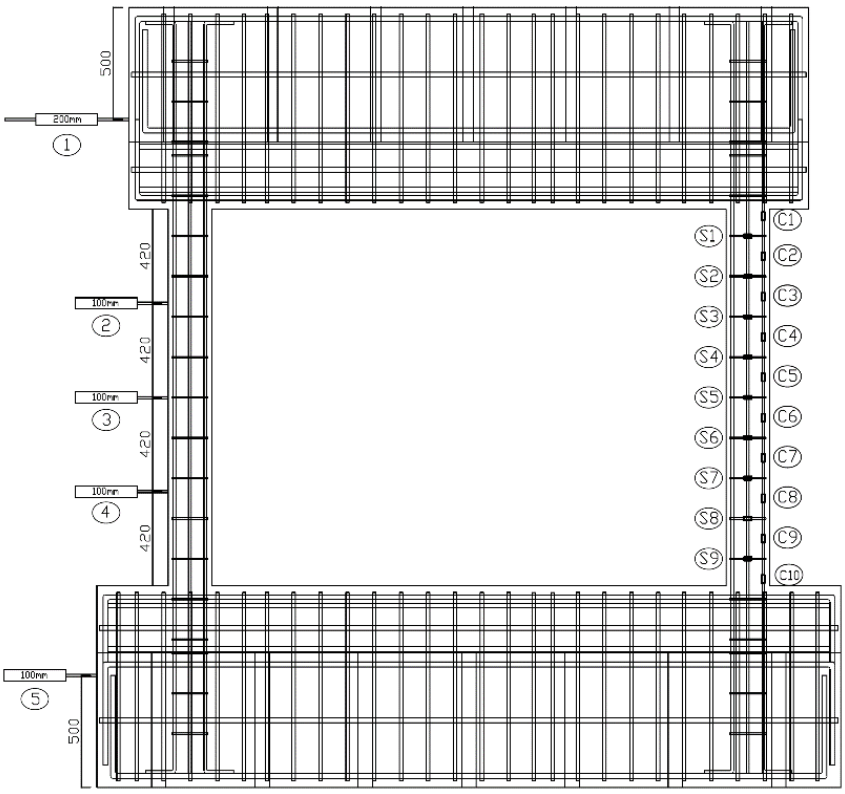

Figure 11. Measurement setup of LVDTs and strain gages.

2.6. Test Results

(1) Load-displacement relationship and strength degradation

Figure 12 shows the hysteretic curves of the system with and without WKDS while Table 3 presents the yield and maximum loads and displacements. When strengthened by WKDS, the maximum load resisting capacity increased from 146.0 kN to 234.0 kN in positive directional loading and from −144.2 kN to −226.9 kN in negative directional loading. As the analytical model estimated that the maximum load would increase from 141.1 kN to 248.5 kN, this suggests that the hysteretic behavior of the Kagome damper can be accurately predicted by the proposed equivalent bi-linear model. Envelopes for each specimen are shown in Figure 13. Figure 14 shows the envelope curve of the Kagome damping device, where it can be seen that the Kagome damper shows stable hysteretic behavior after yielding.

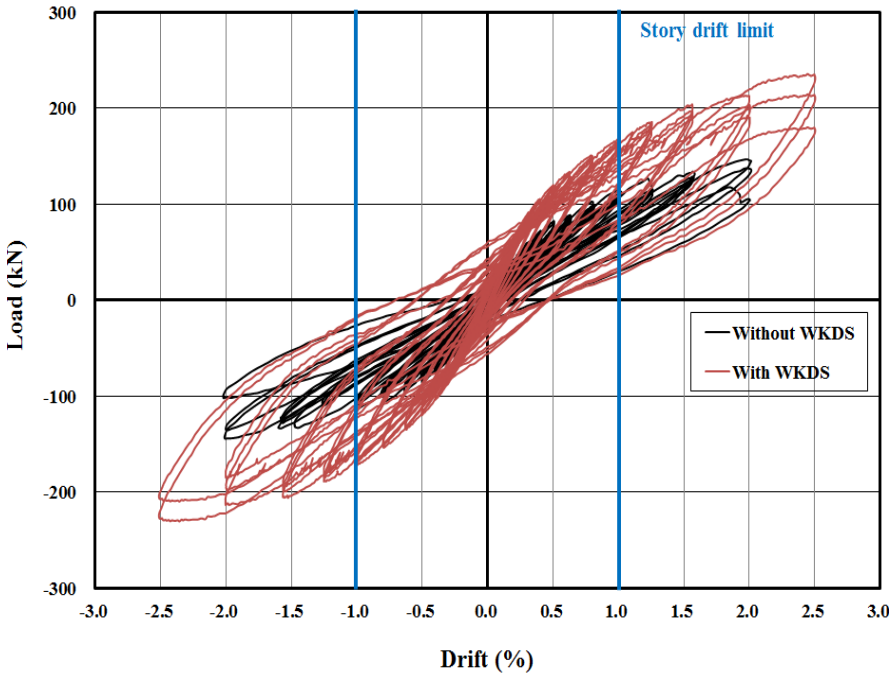

Figure 12. Hysteretic curves of the RC frames with and without the WKDS.

Table 3. Yields and maximum loads and displacements of the RC frames with and without the WKDS.

Specimen	Loading Direction	Yield Load (kN)	Yield Displacement (δy, mm)	Maximum Load (kN)	Maximum Displacement (δmax, mm)
Without WKDS	+	82.7	8.4	146.9	33.6
	–	−85.2	−8.4	−144.2	−33.6
With WKDS	+	107.0	8.4	234.0	42.0
	–	−106.6	−8.4	−226.9	−42.0

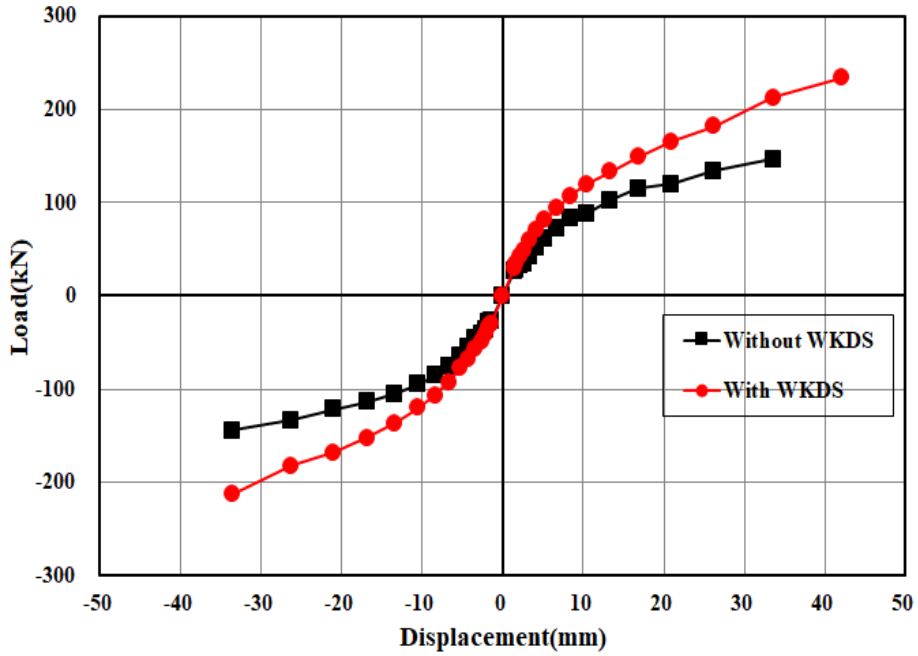

Figure 13. Load–displacement relationship.

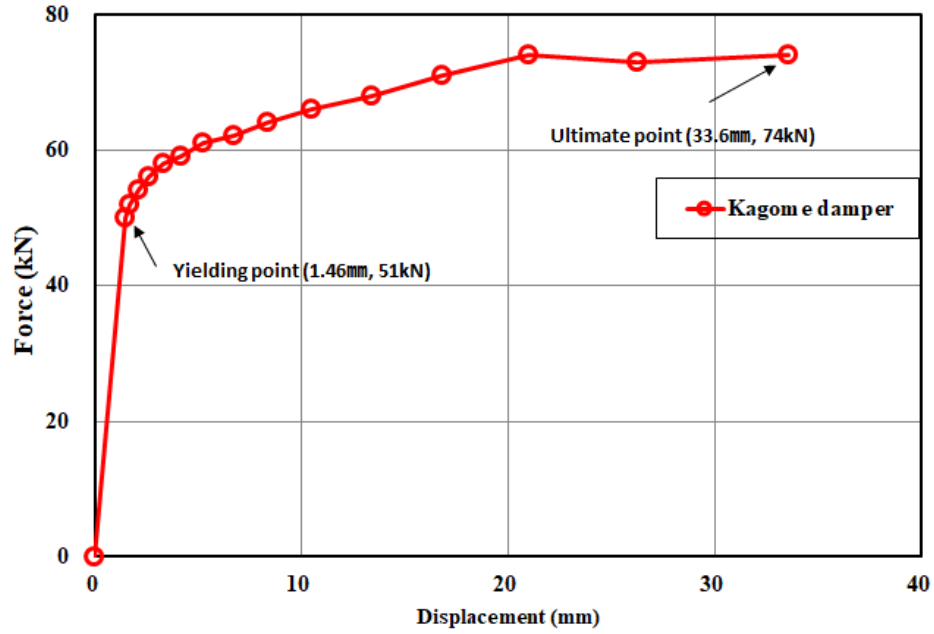

Figure 14. Load–displacement relationship of Kagome damper.

Figure 15 displays the ratios of the maximum strengths at the second and third cycles to the maximum strength at the first cycle. It should be noted that about 8~10% strength degradation of the unreinforced system due to the repeated loading was observed when the lateral displacement exceeded 16.8 mm (1% drift ratio). The strength of the unreinforced system decreased by 70% of the maximum force at the lateral displacement of 33.6 mm (2% drift ratio).

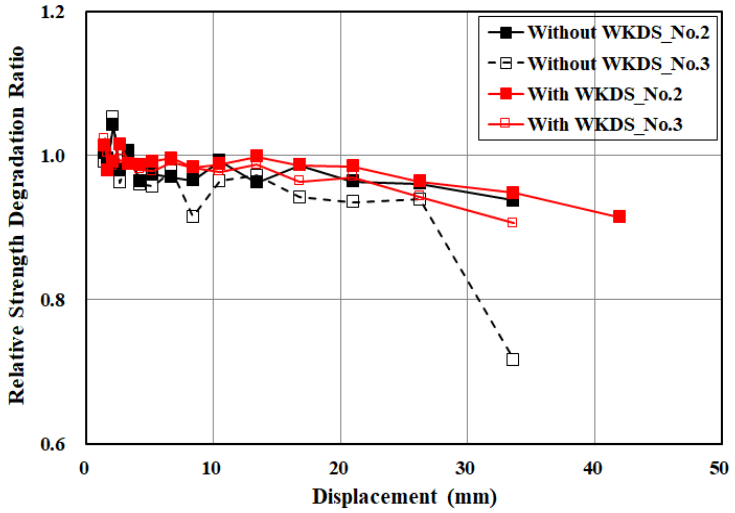

(**a**)

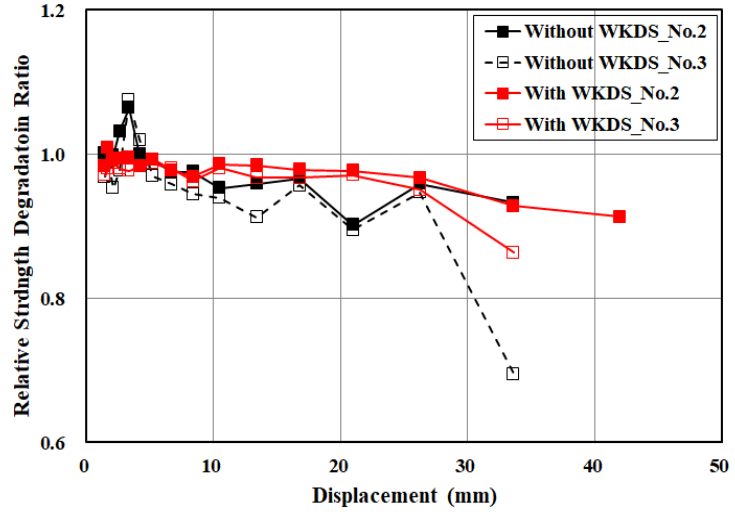

(**b**)

Figure 15. Strength degradation ratios in repeated loadings. (**a**) Loading in positive direction, (**b**) Loading in negative direction.

The strength degradation of the strengthened RC frame with WKDS was not observed at the drift ratio of 1%, with which the unreinforced system showed a substantial decrease in strength. Instead, strength degradation started at the displacement of 26.25 mm and the strength decreased by 90% of the maximum force.

(2) Failure Mode

Figures 16 and 17 show the sequential failure of the specimens while testing. It can clearly be seen that the upper part of the left column of the RC frame without the WKDS was crushed completely, while no notable failure was not observed in the frame with the WKDS.



(**a**) (**b**) (**c**) (**d**)

Figure 16. Failure sequence of the RC frame without the WKDS (upper-left corner). (**a**) 8 Cycle (0.40%), (**b**) 12 Cycle (1.00%), (**c**) 14 Cycle (1.56%), (**d**) final.



(**a**) (**b**) (**c**) (**d**)

Figure 17. Failure sequence of the RC frame with the WKDS (upper-left corner). (**a**) 8 Cycle (0.40%), (**b**) 12 Cycle (1.00%), (**c**) 14 Cycle (1.56%), (**d**) final.

Without WKDS, the first micro flexural cracks were observed at the lower part of the column as the lateral displacement reached 1.68 mm, which corresponds to a 0.1% drift ratio. As the lateral displacement increased, the crack width in the column ends increased and the flexural crack propagated to the middle part of the column. The cracks in the column ends ultimately exhibited the shear crack pattern as the lateral displacement reached 26.25 mm. Shear failure occurred in the upper part of the left column at 33.6 mm displacement and the strength was degraded by approximately 70% of the maximum resisting capacity. The first micro flexural crack of the reinforced system was observed when the lateral displacement reached 2.1 mm. The crack propagation pattern of the system was similar to that of the unreinforced system, but the widths and lengths of the cracks were much smaller than those of the unreinforced frame at the same lateral displacement. The strength consistently increased until the lateral displacement reached 42.0 mm for the first cycle, after which the strength degradation occurred at the second cycle of the loading.

(3) Energy Dissipation Capacity

The cumulated dissipated energy E_D over the loading cycles was calculated using the following equation.

$$E_D = \sum_{i=1}^{N} F(x_i)\Delta x_i, \tag{6}$$

where, $F(x_i)$ and Δx_i are respectively the force and the displacement increment at the i-th loading step.

Figure 18a illustrates the area of energy dissipation. Moreover, Figure 18b represents the ratio of the ED of the unreinforced frame to that of the one reinforced with WKDS. The figures clearly indicate that the WKDS significantly increased the energy dissipation capacity. The mean value of 2.11 in Figure 18b indicates that the energy dissipation capacity of the specimen was doubled when WKDS was adopted.

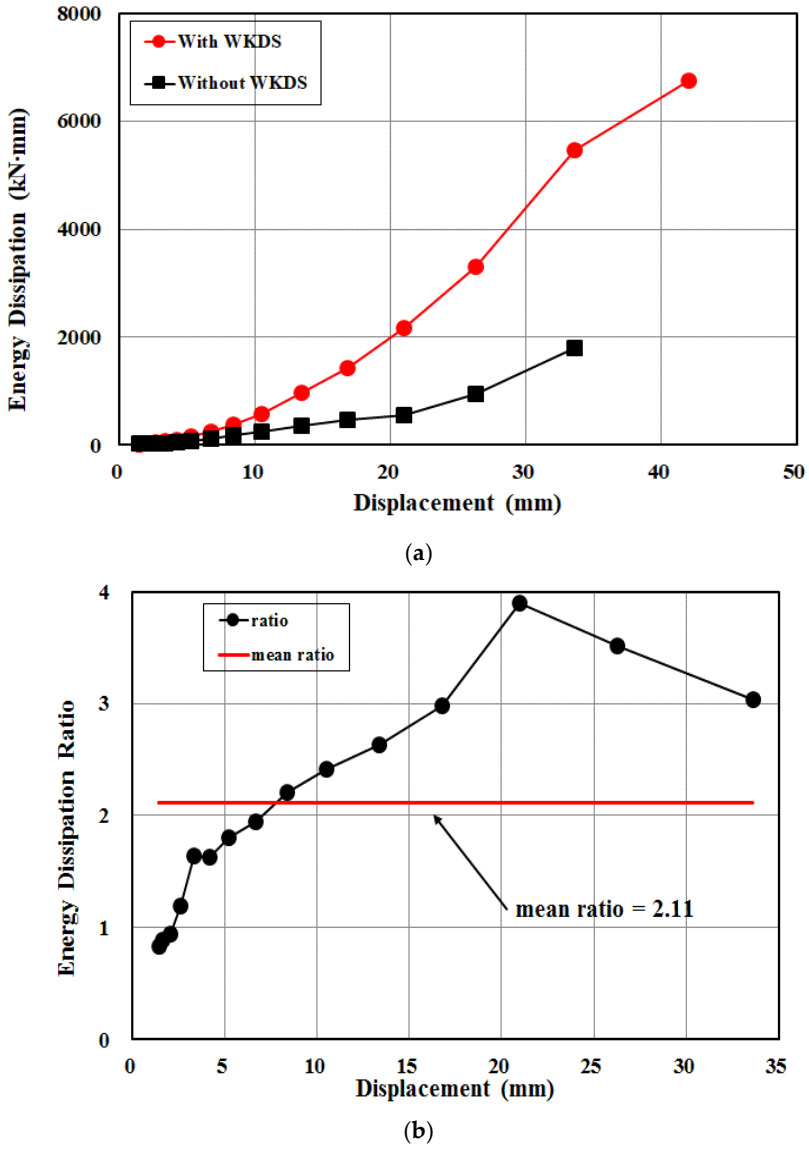

Figure 18. Energy dissipation of specimens. (**a**) Variation of $E_{D,}$ (**b**) Ratio of the E_D.

(4) Strain of the steel bars

Figure 19 shows the strain of the main steel bars in both the unreinforced frame and the frame reinforced with WKDS. The figure shows that the strain of the main bars in the unreinforced frame was much higher than that of the strengthened frame. Most bars in the unreinforced RC yielded a yield strain over 0.0012, while most steel bars except for the steel bars near the bottom end (those strain gages referred to as C9 and C10) did not yield with WKDS.

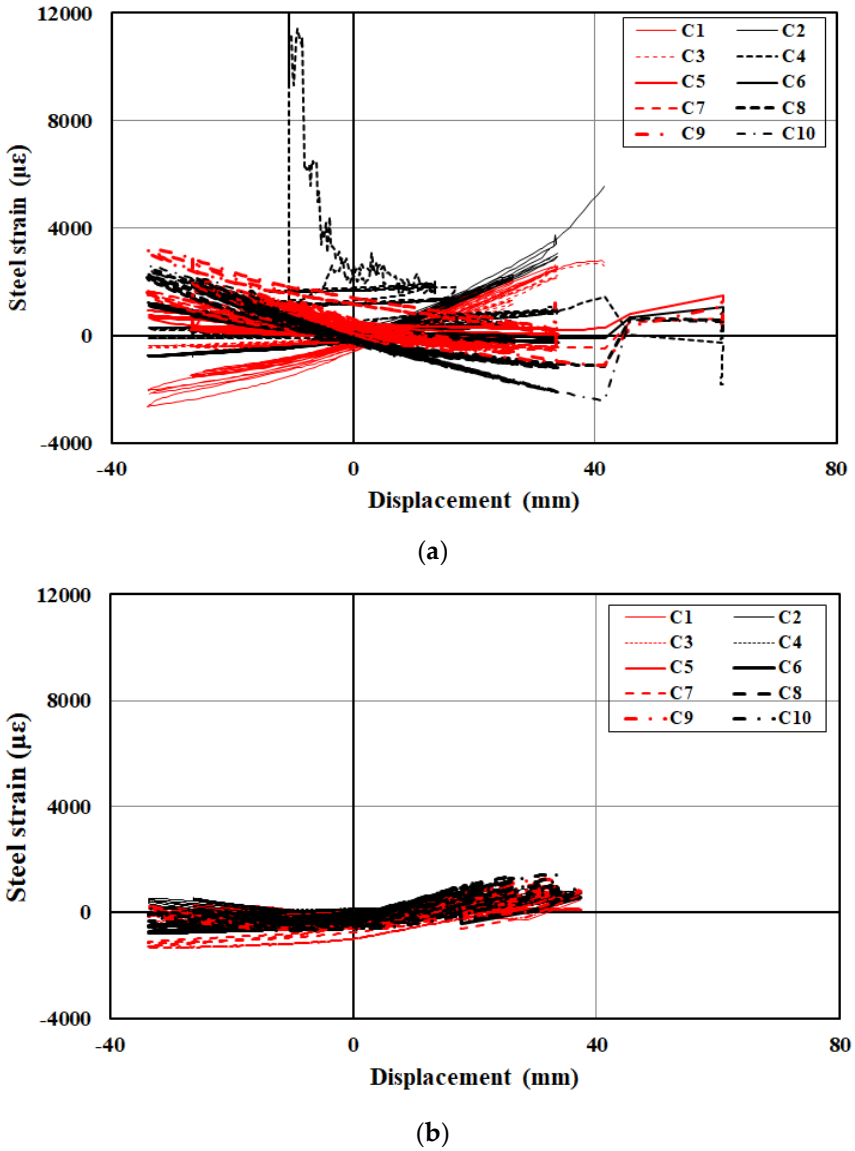

Figure 19. Strain of the main steel bars. (**a**) Without WKDS, (**b**) With WKDS.

3. Analytical Study

3.1. Building Model

To verify the effectiveness of the WKDS in reducing the seismic responses of building structures, an existing four-story RC school building is modelled for a numerical study. The effective ground acceleration is equal to 0.146 g for a design-based earthquake (DBE) and to 0.22 g for a maximum credible earthquake (MCE), while the site class is D.

Figure 20 shows the architectural plan and the location of the WKDS. As can be seen in the plan view, the original building has stiffness irregularity, such that the WKDS were only installed in the frames in the front wall to reduce the irregularity. Nonlinear static and dynamic analyses were conducted, and the plastic hinge properties of the RC members were determined according to ASCE/SEI41-17 [30]. The numerical model was modeled with PERFORM-3D (VER 7.0), which considers the hinge properties of members. The result of the preliminary analysis shows that the building has sound seismic resistant capacity in the y-direction, such that the retrofit using the WKDS was only considered for the x-direction. Therefore, it was determined that the masonry walls should be in the y-direction to confirm the seismic performance. The modeling of the Kagome damper was modeled in a bi-linear manner using the results of a previous study [29] as well as the results of this experiment. Figure 21 shows the hinge properties of columns and beams. The hinge

property details of the members are shown in Table 4. For this building, we review whether it satisfies Lift Safety (LS) in Design Based Earthquake (DBE) level and Collapse Prevention (CP) in Maximum Considered Earthquake (MCE) level.

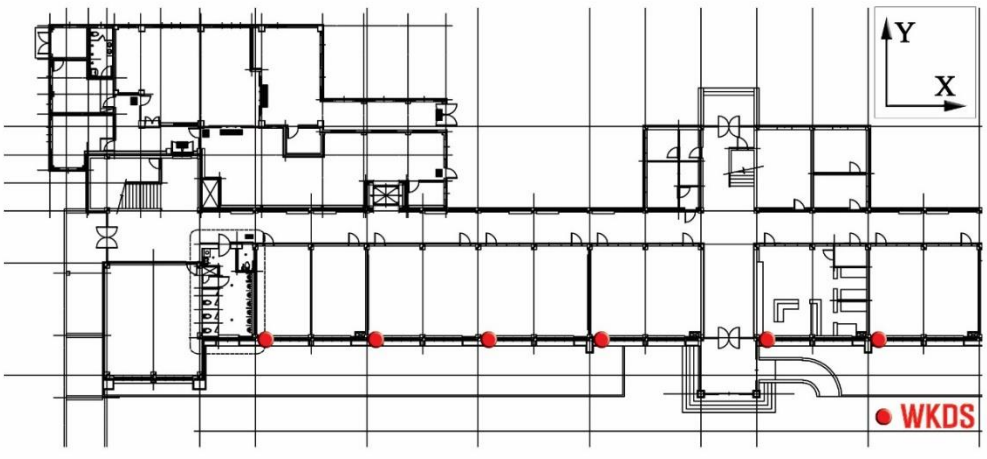

Figure 20. Architectural plan of a building model and location of strengthening with the WKDS.

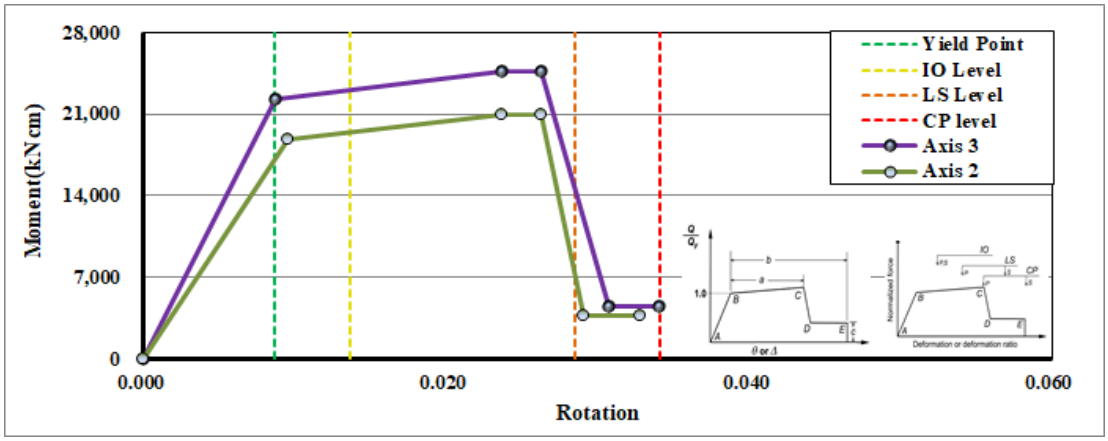

(**a**)

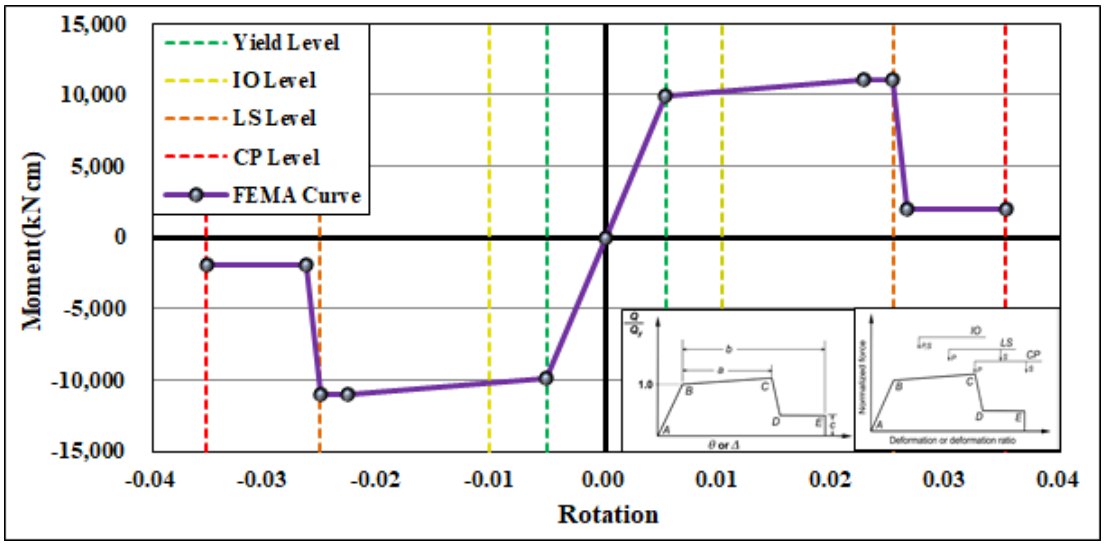

(**b**)

Figure 21. Hinge property of elements. (**a**) Column, (**b**) Girder.

Table 4. Hinge Properties Detail of a Member.

Element		a	b	c	IO	LS	CP
Column (350 × 400 mm)	Axis 3	0.032	0.060	0.20	0.005	0.045	0.060
	Axis 2	0.032	0.060	0.20	0.005	0.045	0.060
Girder (350 × 400 mm)	Upper	0.032	0.060	0.20	0.005	0.045	0.060
	Bottom	0.032	0.060	0.20	0.005	0.045	0.060

3.2. Nonlinear Static Analysis

Figure 22 shows the pushover curves of the unreinforced and the retrofitted building structures. The performance point was obtained using the linearization method presented by FEMA 440 [31].

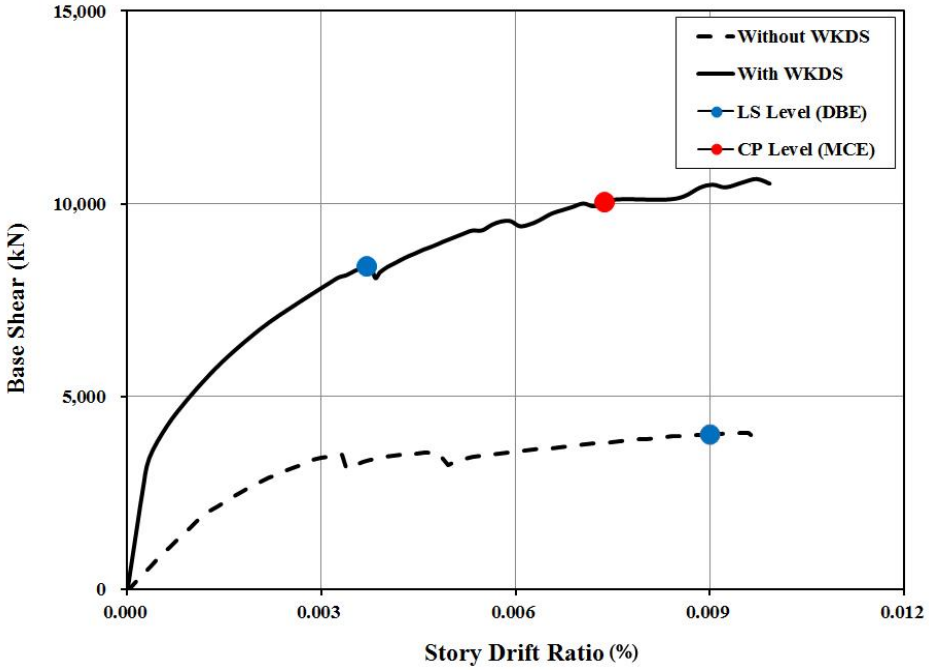

Figure 22. Pushover curves of the unreinforced and the retrofitted building structures with WKDS.

Six WKDSs were installed in each of the first and second floors. As shown in Figure 22, the stiffness and strength significantly increased following installation of the WKDS. The performance point of the original building was 0.008 for the DBE while it was not found for the MCE. The drift ratios at the performance points of the retrofitted structure were 0.0037 for the DBE and 0.0074 for the MCE. These small drift ratios indicate that WKDS effectively minimizes seismic damages to the building structure.

3.3. Nonlinear Dynamic Analysis

3.3.1. Earthquake Records

The site condition of the measured site is bedrock ($V_{s,30}$ > 760 m/s), and in this study, we selected three pairs of bedrock earthquake records and four pairs of artificial earthquake records, which have a 0.3–3.0 scale factor on the bedrock spectrum. Those satisfying the design response spectrum (1.3 times of 90% of the design response spectrum) was scaled satisfactorily. The primary vibration mode shape of the building appeared to be 0.82 s. Figure 23 shows the response spectrum of the design-based earthquake (DBE) of the seismic waves used in the analysis as well as the acceleration time history of each seismic wave.

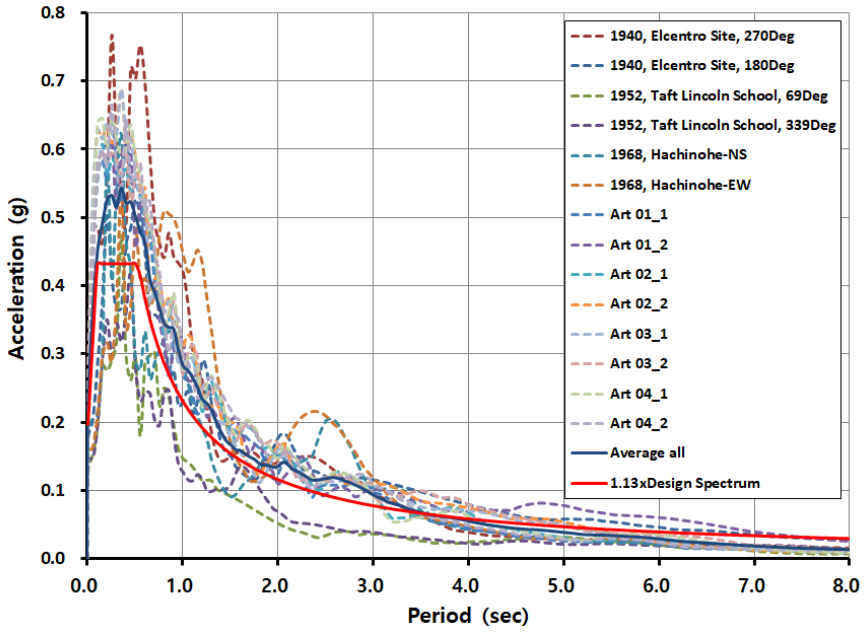

Figure 23. Spectral acceleration responses of the scaled ground accelerations.

3.3.2. Result of Nonlinear Time-History Analysis

Figure 24 shows the structural responses of the unreinforced and retrofitted structures. The peak displacement, acceleration, base shear, and drift ratio values are listed in Table 5. The results were obtained by averaging the results from each seismic load. It can clearly be seen that the drift and displacement of the strengthened structure using WKDS decreased by 50% of the unreinforced structure. The reductions of the absolute acceleration and the base shear were not as large as the displacement response reduction since the building was stiffened and strengthened by the WKDS.

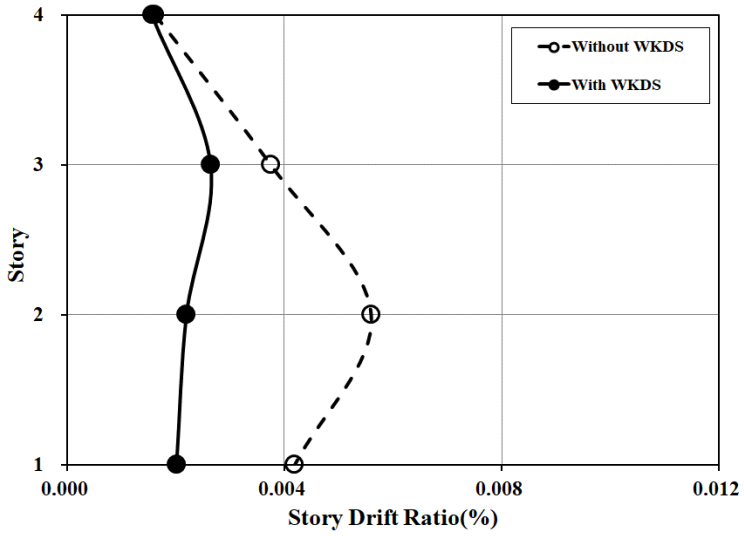

(a)

Figure 24. *Cont.*

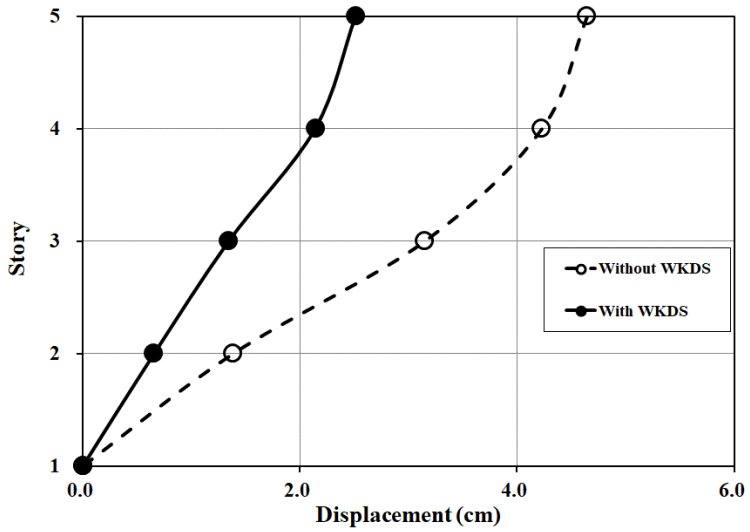

(**b**)

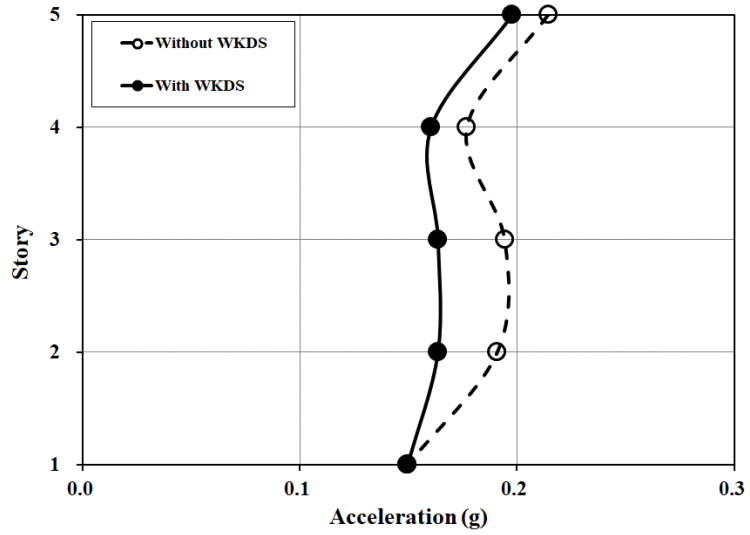

(**c**)

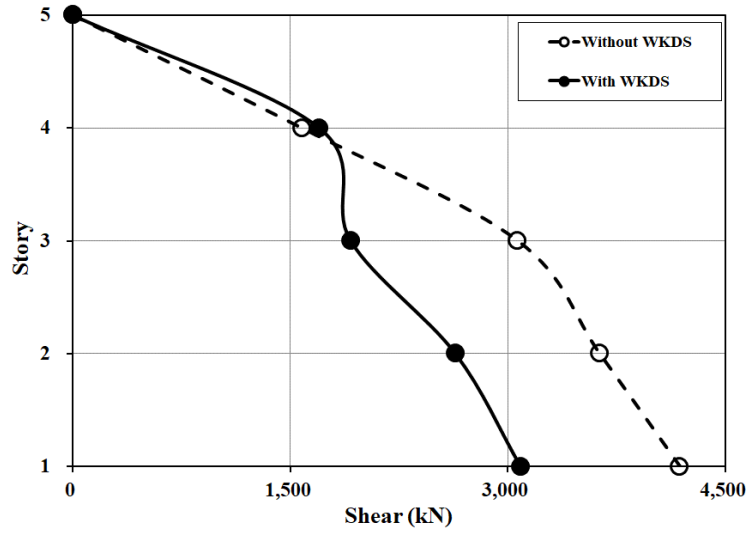

(**d**)

Figure 24. Responses of the unreinforced and the retrofitted structures with WKDS. (**a**) Story drift ratio, (**b**) Maximum displacement, (**c**) Maximum acceleration, (**d**) Story shear.

Table 5. Structural responses from nonlinear dynamic analysis.

Building	Displacement	Acceleration	Shear (kN)	Drift Ratio
Without WKDS (a)	46.4 mm	0.214 g	4185 kN	0.0056
With WKDS (b)	25.2 mm	0.198 g	3088 kN	0.0026
Reduction Ratio (b/a)	0.54	0.92	0.74	0.47

Figures 25 and 26 illustrate shows the hinge properties of the building. The results of the hinge properties show the effect of seismic performance of WKDS.

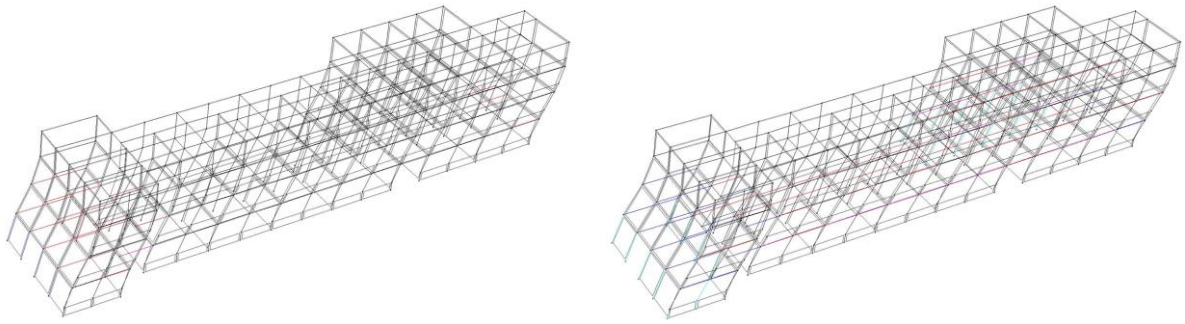

(**a**) (**b**)

Figure 25. Hinge properties without WKDS. (**a**) DBE level, (**b**) MCE level.

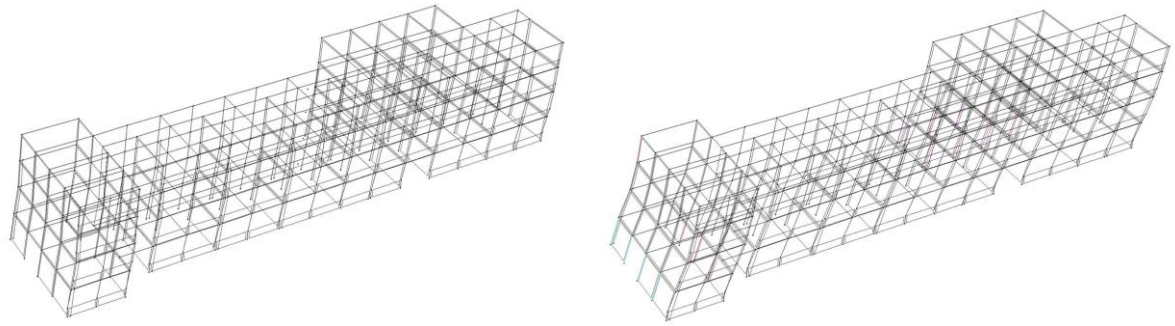

(**a**) (**b**)

Figure 26. Hinge properties with WKDS. (**a**) DBE level, (**b**) MCE level.

Figures 27 and 28 illustrate the hysteretic curves of the six WKDSs installed in the first floor. The diagrams explicitly show that the WKDS adopted in every seismic event effectively dissipates the structural energy.

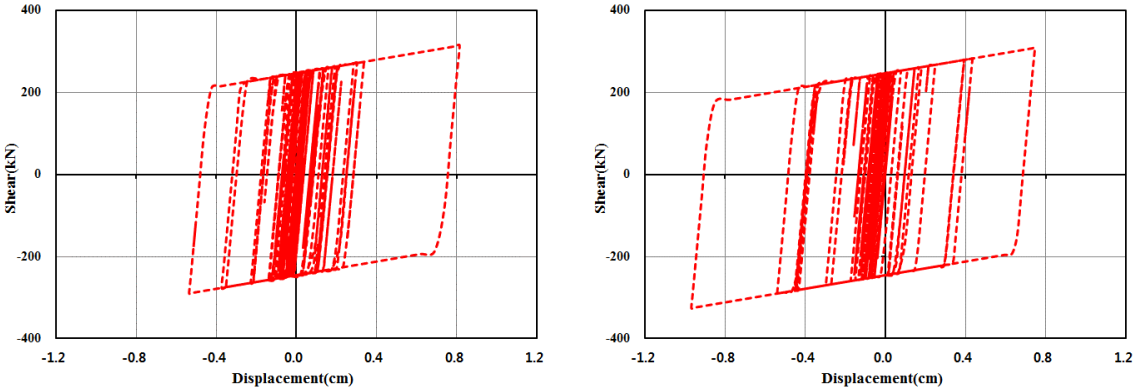

Figure 27. Hysteretic curves of the WKDS (El-Centro EW, 1F).

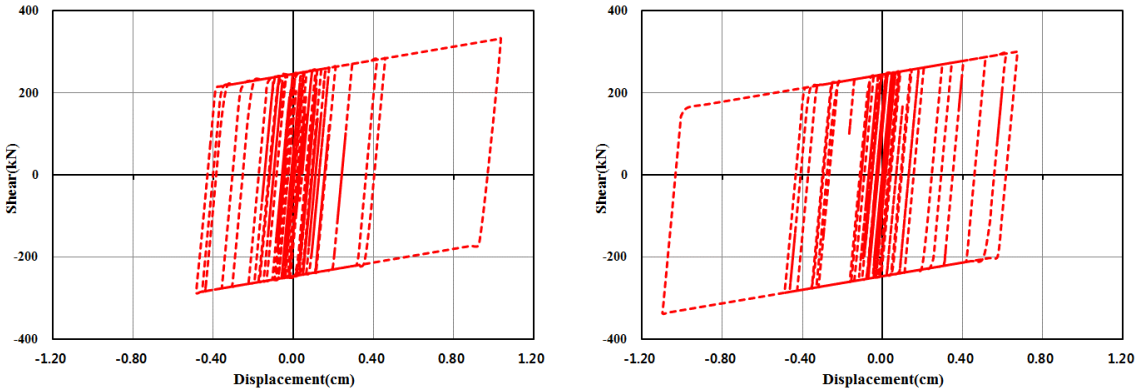

Figure 28. Hysteretic curves of the WKDS (El-Centro EW, 2F).

4. Concluding Remarks

In this study, the applicability of the Kagome truss damper for seismic strengthening to existing RC buildings was discussed and a wall-type Kagome damping system (WKDS) was proposed. The effect of improving seismic performance by applying the proposed WKDS to non-reinforced frames was verified through cyclic loading test. Additionally, nonlinear dynamic analysis was carried out to evaluate the performance of WKDS. Based on the conclusions drawn in the present paper, the following results were obtained:

1. The results of cyclic loading test results indicate that both the stiffness and the strength of a RC frame structure could effectively be enhanced by the WKDS. The unreinforced structure suffered brittle shear failure at the end of the column at 2.0% as a drift ratio, while the retrofitted structure by the WKDS still had been dissipating energy stably by the same drift ratio. The maximal resisting lateral load of the retrofitted structure, as predicted in the numerical analysis, was increased by 1.5 times higher than that of the unreinforced structure. Ultimately, the results suggest that the WKDS is an effective apparatus to mitigate strength degradation improving energy dissipation capacity;
2. It was analytically verified in the nonlinear static and dynamic analyses that the WKDS suppresses the seismic response of the building structure owing to its hysteretic characteristics, as identified in the cyclic loading test. Specifically, the WKDS effectively reduces the drift and displacement responses of the RC frame such that damage of existing buildings can be mitigated substantially even in cases of severe seismic events;
3. In a numerical study of an existing four-story RC school building to verify the efficacy of WKDSs in reducing the seismic responses of building structures, it was clear that the drift and displacement of the structure rehabilitated by using WKDSs reduced by 50% of those of the unreinforced structure. The reductions of the absolute acceleration

and the base shear were not as large as the displacement response reduction since the building was stiffened and strengthened by the WKDS.

Author Contributions: Conceptualization, M.-W.H. and S.-H.L.; methodology, M.-W.H. and S.-H.L.; validation, M.-W.H., Y.L., M.-J.J. and S.-H.L.; formal analysis, M.-W.H., Y.L., M.-J.J. and S.-H.L.; investigation, Y.L., M.-J.J. and M.-W.H.; test, M.-W.H., Y.L., M.-J.J. and S.-H.L.; resources, M.-W.H. and S.-H.L.; data curation, M.-W.H., Y.L., M.-J.J. and S.-H.L.; writing—original draft preparation, S.-H.L.; writing—review and editing, M.-W.H. and S.-H.L.; visualization, S.-H.L. and M.-W.H.; supervision, S.-H.L.; project administration, M.-W.H.; project administration, M.-W.H. and S.-H.L. All authors have read and agreed to the published version of the manuscript.

Funding: This work was supported by Basic Science Research Program through the national Research Foundation of Korea (NRF-2018R1A6A1A07025819, NRF-2018R1D1A1B07048570).

Data Availability Statement: The data used to support the results in this research are included within the article. Furthermore, some of the data in this article are supported by the references mentioned in the paper. If you have any queries regarding the data, the data of this research will be available from the corresponding author upon request.

Conflicts of Interest: The authors declare that there is no conflict of interest regarding the publication of this paper.

References

1. Tsionis, G.; Bossi, A.; Pinto, A.; Marazzi, F. The L'Aquila, Italy Earthquake of 6 April 2009. In *Earthquake Engineering Report 2009*; Institute for the Protection and Security of the Citizen: Ispra, Italy, 2011.
2. Zhao, B.; Taucer, F.; Rossettob, T. Field investigation on the performance of building structures during the 12 May 2008 Wenchuan earthquake in China. *Eng. Struct.* **2009**, *31*, 1707–1723. [CrossRef]
3. Sezen, H.; Elwood, K.J.; Whittaker, A.S.; Mosalan, K.M.; Wallace, J.W.; Stanton, J.F. *Structural Engineering Reconnaissance of the August 17, 1999 Earthquake: Kocaeli (Izmit), Turkey*; Technical Report; Pacific Engineering Research Center, University of California: Berkeley, CA, USA, 2000.
4. Tsai, K.C.; Hsiao, C.P.; Bruneau, M. Overview of Building Damages in 921 Chi-Chi Earthquake. *Earthq. Eng. Eng. Seismol.* **2000**, *2*, 93–108.
5. Verderame, G.M.; de Luca, F.; Ricci, P.; Manfredi, G. Preliminary analysis of a soft-story mechanism after the 2011 L'Aquila earthquake. *Earthq. Eng. Struct. Dyn.* **2011**, *40*, 925–944. [CrossRef]
6. Skinner, R.I.; Kelly, J.M.; Heine, A.J. Hysteretic dampers for earthquake-resistant structures. *Earthq. Eng. Struct. Dyn.* **1974**, *3*, 287–296. [CrossRef]
7. Whittaker, A.S.; Bertero, V.V.; Thompson, C.L.; Alonso, L.J. Seismic Testing of Steel Plate Energy Dissipation Devices. *Earthq. Spectra* **1991**, *7*, 563–604. [CrossRef]
8. Tsai, K.C.; Chen, H.-W.; Hong, C.C.; Su, Y.F. Design of Steel Triangular Plate Energy Absorbers for Seismic-Resistant Construction. *Earthq. Spectra* **1993**, *9*, 505–528. [CrossRef]
9. Benavent, C.A.; Oh, S.H.; Akiyama, H. Ultimate energy absorption capacity of slit-type steel plates subjected to shear deformation. *J. Struct. Constr. Eng.* **1998**, *503*, 139–147. [CrossRef]
10. Bincy, V.; Usha, S. Seismic performance evaluation of steel building frames with modified dual-pipe damper. *IOP Conf. Ser. Mater. Sci. Eng.* **2021**, *1114*, 012004. [CrossRef]
11. Saingam, P.; Sutcu, F.; Terazawa, Y.; Celik, O.C.; Takeuchi, T. Seismic Retrofit of RC Buildings with Viscous Dampers and Elastic Steel Frames including Effect of Composite Behavior. *J. Struct. Eng. B* **2021**, *67*, 569–580.
12. Idels, O.; Lavan, O. Optimization-based seismic design of steel moment-resisting frames with nonlinear viscous dampers. *Struct. Control Health Monit.* **2021**, *28*, e2655. [CrossRef]
13. Taiyari, F.; Mazzolani, F.M.; Bagheri, S. A proposal for energy dissipative braces with U-shaped steel strips. *J. Constr. Steel Res.* **2019**, *154*, 110–122. [CrossRef]
14. Lin, X.; Wu, K.; Skalomenos, K.A.; Lu, L.; Zhao, S. Development of a buckling-restrained shear panel damper with demountable steel-concrete composite restrainers. *Soil Dyn. Earthq. Eng.* **2019**, *118*, 221–230. [CrossRef]
15. Yamazaki, S.; Usami, T.; Nonaka, T. Developing a new hysteretic type seismic damper (BRRP) for steel bridges. *Eng. Struct.* **2016**, *124*, 286–301. [CrossRef]
16. Tagawa, H.; Yamanishi, T.; Takaki, A.; Chan, R.W.K. Cyclic behavior of seesaw energy dissipation system with steel slit dampers. *J. Constr. Steel Res.* **2016**, *117*, 24–34. [CrossRef]
17. Chan, R.W.K.; Yuen, J.K.K.; Lee, E.W.M.; Arashpour, M. Application of Nonlinear-Autoregressive-Exogenous model to predict the hysteretic behaviour of passive control systems. *Eng. Struct.* **2015**, *85*, 1–10. [CrossRef]

18. Infanti, S.; Papanikolas, P.; Benzoni, G.; Castellano, M.G. RION-ANTIRION bridge: Design and full-scale testing of the seismic protection devices. In Proceedings of the 13th World Conference on Earthquake Engineering, Vancouver, BC, Canada, 1–6 August 2004.
19. Milani, A.S.; Dieleli, M. Systematic development of a new hysteretic damper based on torsional yielding: Part-I—Design and development. *Earthq. Eng. Struct. Dyn.* **2015**, *45*, 845–867. [CrossRef]
20. Wadley, H.N.G.; Fleck, N.A.; Evans, A.G. Fabrication and structural performance of periodic cellular metal sandwich structures. *Compos. Sci. Technol.* **2003**, *63*, 2331–2343. [CrossRef]
21. Kang, K.J. *Development of Production Technology of Truss Type Periodic Cellular Metal*; National Designated Laboratory Project, Korea Science and Engineering Foundation: Daejeon, Korea, 2011.
22. Lee, B.K.; Kang, K.J. A parametric study on compressive characteristics of Wire-woven bulk Kagome truss cores. *Compos. Struct.* **2010**, *92*, 445–453.
23. Lee, B.K.; Choi, J.E.; Jeon, I.S.; Kang, K.J. Analysis of Compressive Characteristics of Wire-woven Bulk Kagome. *J. Korean Soc. Mech. Eng.* **2008**, *32*, 70–76. [CrossRef]
24. Lee, M.J. Compressive Characteristics of Two New Types of Periodic Cellular Metals. Master's Thesis, Graduate School, Chonnam National University, Gwangju, Korea, August 2009.
25. Park, J.S.; Joo, J.H.; Lee, B.C.; Kanf, K.J. Mechanical behaviour of tube-woven Kagome truss cores under compression. *Int. J. Mech. Sci.* **2010**, *53*, 65–73. [CrossRef]
26. Lee, Y.H.; Kang, K.J. An Optimal Design of Sandwich Panels with Wire-woven Bulk Kagome Cores. *J. Korean Soc. Mech. Eng.* **2008**, *32*, 782–787. [CrossRef]
27. Hwang, J.S.; Lee, K.S. Seismic Strengthening Effects Based on Pseudodynamic Testing of a Reinforced Concrete Building Retrofitted with a Wire-Woven Bulk Kagome Truss Damper. *Shock. Vib.* **2016**, *2016*, 3956126. [CrossRef]
28. Hwang, J.S.; Lee, K.S.; Hur, M.W.; Lee, S.H. Mechanical hysteresis model of a metal-wire Kagome truss for seismic strengthening for building systems. *J. Asian Archit. Build. Eng.* **2019**, *18*, 112–120. [CrossRef]
29. Beak, E.L.; Oh, S.H.; Lee, S.H. Seismic performance of an Existing Low-Rise Reinforced Concrete Piloti Building Retrofitted by Steel Rod Damper. *J. Earthq. Eng. Soc. Korea* **2014**, *18*, 241–251. [CrossRef]
30. ASCE. *ASCE/SEI 41-17. Seismic Evaluation and Retrofit of Existing Buildings*; American Society of Civil Engineers: Reston, VA, USA, 2017.
31. Applied Technology Council. *Improvement of Static Seismic Analysis Procedures*; FEMA 440 Report 2005; Applied Technology Council: Redwood City, CA, USA, 2005.